Ferrocene−Phenothiazine Conjugated Molecules: Synthesis, Structural Characterization, Electronic Properties, and DFT-TDDFT Computational Study

Wen-Wei Zhang,* Yong-Guang Yu, Zhen-Da Lu, Wei-Li Mao, Yi-Zhi Li, and Qing-Jin Meng*

Institute of Coordination Chemistry, State Key Laboratory of Coordination Chemistry, School of Chemistry and Chemical Engineering, Nanjing University, Nanjing 210093, People's Republic of China

Received October 8, 2006

Two novel Fc−MPT conjugated compounds, 3-(ferrocenylethynyl)-10-methylphenothiazine (**1**) and 3,7-bis(ferrocenylethynyl)-10-methylphenothiazine (**2**), have been synthesized by Sonogashira cross-coupling reactions. Single-crystal X-ray diffraction shows that **2** displays better coplanarity between the Fc and MPT subunits. The crystal packing reveals that **1** stacks in the same direction between the neighboring molecules by the S···H−C (of the Fc moiety) hydrogen bonds, while **2** stacks in an inverse fashion between the adjacent molecules, not only by the S···H−C (of the MPT moiety) hydrogen bonds but also by $\pi\cdots\pi$ interactions. Both complexes show MLCT, ICT, and $\pi \rightarrow \pi^*$ transitions in the UV−visible range in solution, and **2** has a tremendous bathochromic shift and shows a higher oscillator strength of the absorption, which has been verified by TDDFT theoretical calculations. DFT calculations explain the electrochemistry of the two complexes and show that the larger conjugative effect in **2** leads to the smaller HOMO−LUMO gap (E_g). The differences between **1** and **2** indicate that the structural and conjugative effects have great influence on the electronic properties of the molecules.

1. Introduction

Compounds with extending conjugated π-electron systems are of importance in a wide variety of applications such as optical, electronic, optoelectronic, and magnetic matericals.[1] Furthermore, they are promising for generating new models for energy and electron transfer as well as for mimicking charge separation.[2] Recently some tailored organometallic groups were introduced into the organic conjugated π-electron systems through molecular engineering in an effort to seek more active materials for molecular electronic wires and molecular devices.[3] Functional building blocks, bridges linking the building units, and the molecular geometry in the conjugated extended π-electron systems have pronounced influence on the electrical and optical properties. Therefore, the synthesis and investigation of novel conjugated molecules are essential for improving the electronic and optoelectronic properties of such materials and further improvement of the performance of these devices.

In this paper, two conjugated reversible redox-active systems, ferrocene and phenothiazine, were used as building blocks and ethynylene was employed as a π-conjugated linker in the construction of the novel conjugated molecules, since the reversible redox systems display electronic bi- or multistability and so are highly competitive as switching functional units and redox-addressable building blocks of single-molecule-based molecular electronics.[4] In particular, ferrocene, an electron-rich group and electronic communicator, plays an important role in generating semiconductor, superconductor, magnetic, NLO, and redox catalyst materials[5] and phenothiazine, an intriguing type of biologically and pharmaceutically active heterocyclic compound well-known as a pharmacophore in tranquilizers, antituberculosis agents, anti-tumor agents, bactericides, etc.,[6] is now widely studied as an electron donor component and electrically conducting charge-transfer composite in materials science

* To whom correspondence should be addressed. Tel: +86-25-83597374. Fax: +86-25-83317761. E-mail: wwzhang@nju.edu.cn (W.-W.Z.).

(1) (a) Carroll, R. L.; Gorman, C. B. *Angew. Chem., Int. Ed.* **2002**, *41*, 4378. (b) Nitzan, A.; Ratner, M. A. *Science* **2003**, *300*, 1384. (c) Elangovan, A.; Kao, K. M.; Yang, S. W.; Chen, Y. L.; Ho, T. I.; Su, O. Y. *J. Org. Chem.* **2005**, *70*, 4460. (d) Marsden, J. A.; Miller, J. J.; Shirtcliff, L. D.; Haley, M. M. *J. Am. Chem. Soc.* **2005**, *127*, 2464.

(2) (a) Knorr, A.; Daub, J. *Angew. Chem., Int. Ed.* **1997**, *36*, 2817. (b) Davis, W. B.; Svec, W. A.; Wasielewski, M. B. *Nature* **1998**, *60*, 396. (c) Giacalone, F.; Segura, J. L.; Mart, N.; Ramey, J.; Guldi, D. M. *Chem. Eur. J.* **2005**, *11*, 4819.

(3) (a) Sikes, H. D.; Smalley, J. F.; Feldberg, S. W. *Science* **2001**, *291*, 1519. (b) Szafert, S.; Gladysz, J. A. *Chem. Rev.* **2003**, *103*, 4175. (c) Ren, T. *Organometallics* **2005**, *24*, 4854. (d) Blum, A. S.; Ren, T.; Parish, D. A.; Trammell, S. A.; Moore, M. H.; Kushmerick, J. G.; Xu, G. L.; Deschamps, J. R.; Pollack, S. K.; Shashidhar, R. *J. Am. Chem. Soc.* **2005**, *127*, 10010.

(4) (a) Petty, M. C.; Bryce, M. R.; Bloor, D. *An Introduction to Molecular Electronics*; Oxford University Press: New York, 1995. (b) Bumm, L. A.; Arnold, J. J.; Cygan, M. T.; Dunbar, T. D.; Burgin, T. P.; Jones, L., II; Allara, D. L.; Tour, J. M.; Weiss, P. S. *Science* **1996**, *271*, 1705. (c) Cygan, M. T.; Dunbar, T. D.; Arnold, J. J.; Bumm, L. A.; Shedlock, N. F.; Burgin, T. P.; Jones, L., II; Allara, D. L.; Tour, J. M.; Weiss, P. S. *J. Am. Chem. Soc.* **1998**, *120*, 2721. (d) Tour, J. M. *Acc. Chem. Res.* **2000**, *33*, 791. (e) Carroll, R. L.; Gorman, C. B. *Angew. Chem.* **2002**, *114*, 4556.

(5) (a) Oriol, L.; Serrano, J. *Adv. Mater.* **1995**, *7*, 348. (b) Connelly, N. G.; Geiger, W. E. *Adv. Organomet. Chem.* **1984**, *23*, 1. (c) Sailer, M.; Rominger, F.; Muller, T. J. J. *J. Organomet. Chem.* **2006**, *691*, 299. (d) Manners, I. *Angew. Chem., Int. Ed. Engl.* **1996**, *35*, 1602. (e) Bunz, U. H. F. *Angew. Chem., Int. Ed. Engl.* **1996**, *35*, 968. (f) Nguyen, P.; Gómez-Elipe, P.; Manners, I. *Chem. Rev.* **1999**, *99*, 1515. (g) Antonelli, E.; Rosi, P.; Lo Sterzo, C.; Viola, E. *J. Organomet. Chem.* **1999**, *578*, 210. (h) Whittall, I. R.; McDonagh, A. M.; Humphrey, M. G.; Samoc, M. *Adv. Organomet. Chem.* **1998**, *43*, 349. (i) Long, N. J. *Angew. Chem., Int. Ed. Engl.* **1995**, *34*, 6. (j) Dhenaut, C.; Ledoux, I.; Samuel, I. D. W.; Zyss, J.; Bourgault, M.; Le Bozec, H. *Nature* **1995**, *374*, 339. (k) Tamm, M.; Grzegorzeweski, A.; Steiner, T.; Jentzsch, T.; Werncke, W. *Organometallics* **1996**, *15*, 4984.

(6) (a) Mietzsch, F. *Angew. Chem.* **1954**, *66*, 363. (b) Ionescu, M.; Mantsch, H. *Adv. Heterocycl. Chem.* **1967**, *8*, 83. (c) Bodea, C.; Silberg, I. *Adv. Heterocycl. Chem.* **1968**, *9*, 321. (d) Okafor, C. O. *Heterocycles* **1977**, *7*, 391. (e) Albery, W. J.; Foulds, A. W.; Hall, K. J.; Hillman, A. R.; Edgell, R. G.; Orchard, A. F. *Nature* **1979**, *282*, 793.

10.1021/om060923o CCC: $37.00
Publication on Web 01/20/2007

Scheme 1. π-Conjugated Ferrocene−Phenothiazine Compounds 1 and 2 by Sonogashira Cross-Coupling Reaction

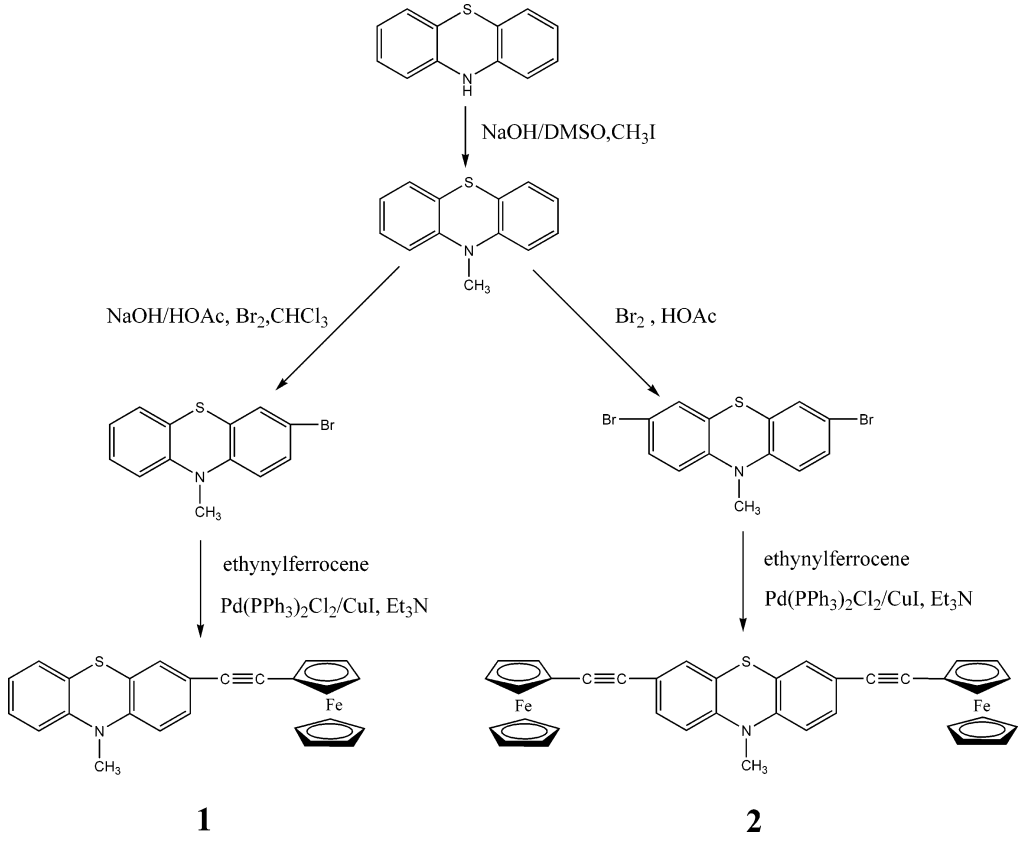

investigations due to its favorable electronic properties.[7] Therefore, in consideration of the above two coupled redox systems integrating into the π-conjugated chains by a conjugated linker, an intense electronic communication between the redox centers may be observed, making a good candidate for redox-addressable molecular wires.

Here, we wish to report the synthesis and characterization of the ferrocenylethynyl-substituted phenothiazines **1** and **2** (see Scheme 1). It is shown that both the electron-rich ferrocenyl unit and the heteroaromatic phenothiazine ring are excellent molecular building blocks for the highly extended π-electron conjugations. Moreover, **1** and **2** have different π-electron conjugative units, which will lead to different electronic structures and variable conjugative degrees. Both the nature of the electronic structure and the conjugative effect influence the electronic properties. Detailed results and discussion are elaborated in the following sections.

2. Experimental Section

2.1. General Procedures. All chemicals were purchased as reagent grade and used without further purification. Dichloromethane, chloroform, methyl cyanide, toluene, dioxane, piperidine, and triethylamine were dried and distilled according to standard procedures. Ethynylferrocene,[8] 10-methylphenothiazine,[9] and 3-bromo-10-methylphenothiazine and 3,7-dibromo-10-methylphenothiazine[10] were prepared according to literature procedures. All of the reactions were monitored by TLC (silica gel plates, GF254). Silica gel 60 (100−200 mesh) was used for column chromatography. Elemental analyses (C, H, and N) were carried out on a Perkin-Elmer 240 analyzer. The IR spectra were obtained as KBr pellets on a VECTOR TM 22 spectrometer with KBr pellets in the 4000−400 cm^{-1} region; the electronic absorption spectra were carried out on a LAMBDA-35 UV/vis spectrophotometer, and ^1H NMR spectra were measured on Bruker AM5600 spectrometers at 298 K using TMS as the internal standard.

2.2. Electrochemical Measurements. Cyclic voltammetric experiments were performed under nitrogen in dry and degassed CH_2Cl_2 at a scan rate of 100 mV s^{-1} with a CHI 660B potentiostatic instrument at room temperature. The three-electrode cell comprises a 1 mm platinum -disk working electrode, a platinum-wire auxiliary electrode, and an Ag/Ag^+ reference electrode. The electrolyte is n-Bu_4NClO_4 (0.1 mol dm^{-3}). Differential pulse voltammetry (DPV) was also done with a CHI 660B instrument with a 50 ms pulse width. The potentials were corrected to the internal standard of Fc/Fc^+ in CH_2Cl_2 (0.072 V vs Ag/Ag^+ electrode).

2.3. Crystallography. Single-crystal X-ray diffraction data were measured on a Bruker SMART APEX CCD diffractometer using graphite-monochromated Mo Kα radiation (λ = 0.710 73 Å) at room temperature using the ψ-scan technique. Cell refinement and data reduction were carried out with the SAINT program. Lorentz−polarization and absorption corrections were applied. The structures were solved by direct methods and refined with the full-matrix least-squares technique using the SHELXS-97 and SHELXL-97 programs.[11] Anisotropic thermal parameters were assigned to all nonhydrogen atoms. Crystallographic refinement parameters of complexes

(7) (a) Wheland, R. C.; Gillson, J. L. *J. Am. Chem. Soc.* **1976**, *98*, 3916. (b) Knorr, A. Daub, *J. Angew. Chem.* **1995**, *107*, 2925. (c) Spreitzer, H.; Scholz, M.; Gescheidt, G.; Daub, J. *Liebigs Ann. Chem.* **1996**, 2069. (d) Spreitzer, H.; Daub, J. *Chem. Eur. J.* **1996**, *2*, 1150. (e) Krämer, C. S.; Müller, T. J. J. *Eur. J. Org. Chem.* **2003**, *18*, 3534.

(8) Rosenblum, M.; Brawn, N.; Papenmeier, J.; Applebaum, M. *J. Organomet. Chem.* **1966**, *6*, 173.

(9) Kim, S. K.; Lee, J. H; Hwang, D. H. *Synth. Met.* **2005**, *152*, 201.

(10) (a) Cymerman-Craig, J.; Rogers, W. P.; Warwick, G. P. *Aust. J. Chem.* **1955**, *8*, 252. (b) Bodea, C.; Terdic, M. *Acad. Rep. Pop. Rom.* **1962**, *13*, 81. [*Chem. Abstr.* **1963**, *59*, 11477b].

(11) (a) Sheldrick, G. M. *SHELXS-97*, Program for X-ray Crystal Structure Solution; University of Göttingen, Göttingen, Germany, 1997. (b) Sheldrick, G. M. *SHELXL-97*, Program for X-ray Crystal Structure Refinement; University of Göttingen, Göttingen, Germany, 1997.

Table 1. Crystallographic Data and Refinement Parameters for 1 and 2·H_2O

	1	**2**·H_2O
empirical formula	$C_{25}H_{19}FeNS$	$C_{37}H_{29}Fe_2NOS$
formula wt	421.32	647.37
cryst syst	triclinic	monoclinic
space group	$P\bar{1}$	$P2_1/c$
a (Å)	9.6412(8)	19.672(2)
b (Å)	9.6605(8)	7.5147(8)
c (Å)	11.047(1)	20.205(2)
α (deg)	95.9980(10)	90.00
β (deg)	108.8210(10)	94.327(2)
γ (deg)	91.0920(10)	90.00
V (Å^3)	967.04(14)	2978.4(5)
Z	2	4
ρ (g cm^{-3})	1.447	1.444
F(000)	436	1336
GOF on F^2	1.053	0.964
R1, wR2[a] ($I > 2\sigma(I)$)	0.0301, 0.0891	0.0566, 0.1164
R1, wR2[a] (all data)	0.0325, 0.0908	0.0871, 0.1225

[a] $R1 = \sum||F_o| - |F_c||/|F_o|$; $wR2 = [\sum w(F_o^2 - F_c^2)^2/\sum w(F_o^2)^2]^{1/2}$.

Table 2. Selected Bond Lengths (Å) and Angles (deg) for 1 and 2·H_2O

	Complex **1**		
C10−C11	1.440(2)	C12−C13	1.436(3)
C11−C12	1.190(3)		
C12−C11−C10	177.2(2)	C9−C10−C11	127.41(17)
C11−C12−C13	176.6(2)	C11−C10−C6	124.91(17)
C14−C13−C12	121.11(17)	C16−N1−C20	119.50(15)
C18−C13−C12	120.66(17)	C17−S1−C25	99.08(8)
	Complex **2**·H_2O		
C10−C11	1.445(5)	C23−C26	1.412(5)
C11−C12	1.149(5)	C26−C27	1.196(5)
C12−C13	1.468(5)	C27−C37	1.445(5)
C12−C11−C10	175.7(4)	C17−S1−C25	99.70(16)
C11−C12−C13	178.4(5)	C27−C26−C23	174.7(4)
C14−C13−C12	121.6(4)	C26−C27−C37	177.1(4)
C18−C13−C12	117.3(3)	C22−C23−C26	118.1(3)
C9−C10−C11	126.6(4)	C24−C23−C26	123.4(4)
C11−C10−C6	125.4(4)	C33−C37−C27	125.1(3)
C16−N1−C20	116.6(3)	C36−C37−C27	126.7(4)

1 and **2** are summarized in Table 1, and selected bond distances and angles of these complexes are given in Table 2.

2.4. Theoretical Methods. All calculations on complexes **1** and **2** were carried out with the Gaussian03 program package[12] by using density functional theory (DFT) and time-dependent DFT (TD-DFT): Becke's three-parameter functional[13] combined with Lee, Yang, and Parr's correlation functional[14] (B3LYP), along with the 6-31G* basis set, was used. Single-point energy calculations of the electronic properties of **1** and **2** at their crystal geometries were carried out by utilizing DFT at the B3LYP/6-31G* level. All of the geometries and electronic properties were calculated by assuming **1** and **2** to be isolated molecules. The lowest 20 singlet−singlet transitions up to a wavelength of ca. 290 nm were computed by TDDFT calculations.

2.5. Synthesis of Complex 1. Under an N_2 atmosphere, a suspension of 3-bromo-10-methylphenothiazine (146.8 mg, 0.5024 mmol) and ethynylferrocene (116.8 mg, 0.5563 mmol), together with bis(triphenylphosphine)palladium(II) dichloride (3.3 mg, 0.0047 mmol) and copper(I) iodide (1.6 mg, 0.0084 mmol) in anhydrous triethylamine (10 mL), was stirred and heated to reflux temperature until complete consumption of the bromide (monitored by TLC). Then the solvent was evaporated under vacuum. The residue was dissolved in dichloromethane, and this solution was washed with water for several times, dried with anhydrous $MgSO_4$, and filtered off. The product in the filtrate was chromatographed on silica gel using dichloromethane−hexane (1/3 v/v) as eluent. The second brown-red band was collected and then evaporated under vacuum to give a brown-red solid. Yield: 110.0 mg (52.4%). Crystals of **1** suitable for an X-ray structural determination were obtained by slow diffusion of hexane into a dichloromethane solution of **1**.

Spectral data of **1**: IR (KBr disk) 2207 cm^{-1} ($\nu_{C\equiv C}$); ^{1}H NMR (500 MHz, CD_3COCD_3): δ 7.33 (d, J = 8.55 Hz, 1H), 7.24 (s, 2H), 7.17 (d, J = 7.50 Hz, 1H), 7.00 (m, 2H), 6.95 (d, J = 8.50 Hz, 1H), 4.50 (s, 2H), 4.30 (s, 2H), 4.26 (s, 5H), 3.43 (s, 3H). Anal. Calcd for $C_{25}H_{19}NSFe$: C, 71.27; H, 4.55; N, 3.32. Found: C, 71.39; H, 4.74; N, 3.17.

2.6. Synthesis of Complex 2. Under an N_2 atmosphere, a suspension of 3,7-dibromo-10-methylphenothiazine (181.0 mg, 0.4891 mmol) and ethynylferrocene (225.6 mg, 1.075 mmol), together with bis(triphenylphosphine)palladium(II) dichloride (3.3 mg, 0.0047 mmol) and copper(I) iodide (1.4 mg, 0.0074 mmol) in anhydrous triethylamine (10 mL), was stirred and refluxed for 4 h until complete consumption of the dibromide (monitored by TLC). Then the solvent was evaporated under vacuum. The residue was dissolved in dichloromethane, and this solution was washed with water several times and then dried with anhydrous $MgSO_4$. After filtration and concentration, the desired product **2** was separated by column chromatography on silica gel using dichloromethane−hexane (1/3 v/v) as eluent. Yield: 129.0 mg (42.1%). Crystals of **2** suitable for an X-ray structural determination were obtained by slow diffusion of hexane into a dichloromethane solution of **2**.

Spectral data of **2**: IR (KBr disk) 2213 cm^{-1} ($\nu_{C\equiv C}$); ^{1}H NMR (500 MHz, $CDCl_3$): δ 7.31 (d, J = 8.45 Hz, 2H), 7.29 (s, 2H), 6.75 (d, J = 8.25 Hz, 2H), 4.51 (s, 4H), 4.27 (s, 14H), 3.40 (s, 3H). Anal. Calcd for $C_{37}H_{27}NSFe_2$: C, 70.64; H, 4.33; N, 2.23. Found: C, 70.55; H, 4.42; N, 2.28.

3. Results and Discussion

3.1. Preparation and Spectroscopic Characterization. Generally, Suzuki cross-coupling, Sonogashira cross-coupling, and Stille cross-coupling reactions are all convenient routes to oligomers with extended π-electron conjugation.[15] Since the bromo-substituted phenothiazine is easily obtained by electrophilic substitution of phenothiazine, and ethynylferrocene, the simplest conjugated member of ferrocene, is also convenient to prepare, we chose the Sonogashira cross-coupling reaction to furnish the π-conjugated ferrocene−phenothiazine electrophores with triethylamine as a base and bis(triphenylphosphine)-

(12) Frisch, M. J.; Trucks, G. W.; Schlegel, H. B.; Scuseria, G. E.; Robb, M. A.; Cheeseman, J. R.; Montgomery, J. A., Jr.; Vreven, T.; Kudin, K. N.; Burant, J. C.; Millam, J. M.; Iyengar, S. S.; Tomasi, J.; Barone, V.; Mennucci, B.; Cossi, M.; Scalmani, G.; Rega, N.; Petersson, G. A.; Nakatsuji, H.; Hada, M.; Ehara, M.; Toyota, K.; Fukuda, R.; Hasegawa, J.; Ishida, M.; Nakajima, T.; Honda, Y.; Kitao, O.; Nakai, H.; Klene, M.; Li, X.; Knox, J. E.; Hratchian, H. P.; Cross, J. B.; Bakken, V.; Adamo, C.; Jaramillo, J.; Gomperts, R.; Stratmann, R. E.; Yazyev, O.; Austin, A. J.; Cammi, R.; Pomelli, C.; Ochterski, J. W.; Ayala, P. Y.; Morokuma, K.; Voth, G. A.; Salvador, P.; Dannenberg, J. J.; Zakrzewski, V. G.; Dapprich, S.; Daniels, A. D.; Strain, M. C.; Farkas, O.; Malick, D. K.; Rabuck, A. D.; Raghavachari, K.; Foresman, J. B.; Ortiz, J. V.; Cui, Q.; Baboul, A. G.; Clifford, S.; Cioslowski, J.; Stefanov, B. B.; Liu, G.; Liashenko, A.; Piskorz, P.; Komaromi, I.; Martin, R. L.; Fox, D. J.; Keith, T.; Al-Laham, M. A.; Peng, C. Y.; Nanayakkara, A.; Challacombe, M.; Gill, P. M. W.; Johnson, B.; Chen, W.; Wong, M. W.; Gonzalez, C.; Pople, J. A. *Gaussian 03*, revision B.04; Gaussian, Inc.: Wallingford, CT, 2004.

(13) Becke, A. D. *J. Chem. Phys.* **1993**, *98*, 5648.

(14) (a) Lee, C.; Yang, W.; Parr, R. G. *Phys. Rev. B* **1988**, *37*, 785. (b) Miehlich, B.; Savin, A.; Stoll, H.; Preuss, H. *Chem. Phys. Lett.* **1989**, *157*, 200.

(15) (a) Erdogan, B.; Song, L. L.; Wilson, J. N.; Park, J. O.; Srinivasarao, M.; Bunz, U. H. F. *J. Am. Chem. Soc.* **2004**, *126*, 3678. (b) Furuta, P.; Brooks, J.; Thompson, M. E.; Frechet, J. M. J. *J. Am. Chem. Soc.* **2003**, *125*, 13165. (c) Batey, R. A.; Shen, M.; Lough, A. J. *Org. Lett.* **2002**, *4*, 1411. (d) Chow, H.-F.; Wan, C.-W.; Low, K.-H.; Yeung, Y.-Y. *J. Org. Chem.* **2001**, *66*, 1910. (e) Liu, C.-Y.; Luh, T.-Y. *Org. Lett.* **2002**, *4*, 4305. (f) Murata, M.; Yamada, M.; Fujita, T.; Kojima, K.; Kurihara, M.; Kubo, K.; Kobayashi, Y.; Nishihara, H. *J. Am. Chem. Soc.* **2001**, *123*, 12903.

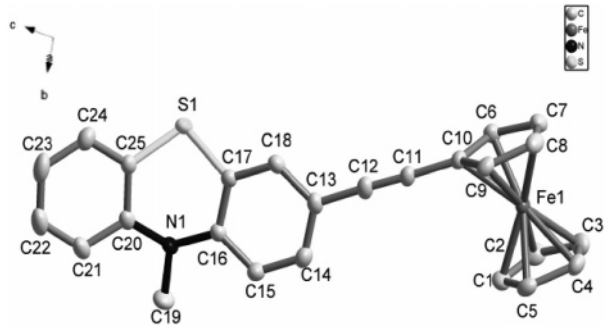

Figure 1. ORTEP diagram of **1** with ellipsoids drawn at the 30% probability level. Hydrogen atoms are omitted for clarity.

palladium(II) and copper(I) iodide as catalysts (Scheme 1). The desired complexes were obtained in good yield.

The IR and ^{1}H NMR spectra unambiguously support the structural assignments of the ferrocene−phenothiazine compounds **1** and **2**. For instance, both **1** and **2** exhibit the characteristic −C≡C− triple-bond stretching vibrations around 2100 cm^{-1}, show the characteristic resonance bands of methylphenothiazine moiety in the 6.7−7.4 ppm range and at about 3.4 ppm, and exhibit the characteristic resonance bands of the ferrocene moiety in the 4.2−4.5 ppm range. Moreover, the analytical data also indicate that the synthesized complexes are in accordance with the predicted molecular structures.

3.2. Structural Characterization. The molecular structures of **1** and **2** are shown in Figures 1 and 2, respectively. The crystallographic data and selected bond lengths and angles are given in Tables 1 and 2, respectively. The X-ray crystal structure analysis clearly shows the characteristic butterfly conformation of the phenothiazine core unit.

Complex **1** crystallizes in the $P\bar{1}$ space group. The −C≡C− bond length is within the expected range (C11−C12 = 1.190 Å), and the −C≡C− bond angle is nearly 180° (C12−C11−C10 = 177.2°; C11−C12−C13 = 176.6°). The dihedral angle of the planes C16−C17−S1−N1 (hc1) and C20−C25−S1−N1 (hc2) is 39.7°, assuming that the atoms C16, C17, S1, N1 and C20, C25, S1, N1 are respectively coplanar (in fact, C16, C17, S1, and N1 are almost coplanar with a small dihedral angle of 1.7°; similarly, C20, C25, S1, and N1 are nearly coplanar with a diheral angle of 1.6°). The benzo ring of C13−C18 (bz1) is tilted from coplanarity with hc1 by 5.0°, and the other benzo ring of C20−C25 (bz2) is tilted from hc2 by 3.5°. The dihedral angle of the two benzo rings is 32.2°. The two Cp rings of the ferrocenyl group are almost parallel to each other (the dihedral angle of Cp1 (C6−C10) and Cp2 (C1−C5) is only 0.1°). The Cp planes and the benzo rings are almost perpendicularly arranged (the angles of bz1 with Cp1 and Cp2 are both 101.6°; the angles of bz2 with Cp1 and Cp2 are 86.8 and 86.7°, respectively). In the crystal packing along the *a* axis (Figure 3), the phenothiazinyl moieties are arranged in the same orientation between neighboring layers with a face-to-face distance of 4.609 Å. Limited π-stacking of the phenothiazines will contribute to the stabilization of the crystal packing, since the phenothiazines cannot be well stacked due to the steric hindrance of the ferrocenyl groups. However, strong C(3)−H(3)···S(1) hydrogen bonds exist between the molecules with S···H separations of 2.887 Å (see the Supporting Information). The hydrogen-bonding interactions play an important role in the supramolecular architecture in the solid state of **1**.

Complex **2** crystallizes in the $P2_1/c$ space group. The two −C≡C− triple-bond lengths are 1.149 Å (C11−C12) and 1.196 Å (C26−C27), lying within the usual range. The −C≡C− bond angle is almost linear (C12−C11−C10 = 175.7°; C11−C12−C13 = 178.4°; C27−C26−C23 = 174.7°; C26−C27−C37 = 177.1°). The dihedral angle of the planes C16−C17−S1−N1 (hc1) and C20−C25−S1−N1 (hc2) is 40.5°, assuming that the atoms C16, C17, S1, N1 and C20, C25, S1, N1 are coplanar, respectively (in fact, C16, C17, S1, and N1 are coplanar and C20, C25, S1, and N1 are almost coplanar with a small dihedral angle of 0.6°). The benzo ring of C13−C18 (bz1) is titled from coplanarity with hc1 by 2.2°, and the other benzo ring of C20−C25 (bz2) is tilted from hc2 by 2.6°. The dihedral angle of the two benzo rings is 35.9°. It can be seen from the data that the coplanarity of the phenothiazinyl moiety in complex **2** is better than that in complex **1**, although the folding angle of the phenothiazinyl group in complex **2** is slightly larger than that in complex **1** by 0.4°. Similarly, the two pairs of Cp rings are nearly parallel to each other (the angle of Cp1 (C6−C10) with Cp2 (C1−C5) is 1.3°, and the angle of Cp3 (C33−C37) with Cp4 (C28−C32) is 0.9°). In comparison with complex **1**, complex **2** displays much smaller dihedral angles of Cp planes and benzo rings. The angles of bz1 with Cp1, Cp2, Cp3, and Cp4 are 52.5, 51.3, 50.3, and 51.2°, respectively, and the angles of bz2 with Cp1, Cp2, Cp3, and Cp4 are 48.1, 46.8, 49.1, and 49.4°, respectively. All of these angles are almost the same. The much smaller angles of Cp planes vs benzo planes in complex **2** further indicate the better coplanarity between the Fc and MPT subunits in **2**. This may result in superior Fc−

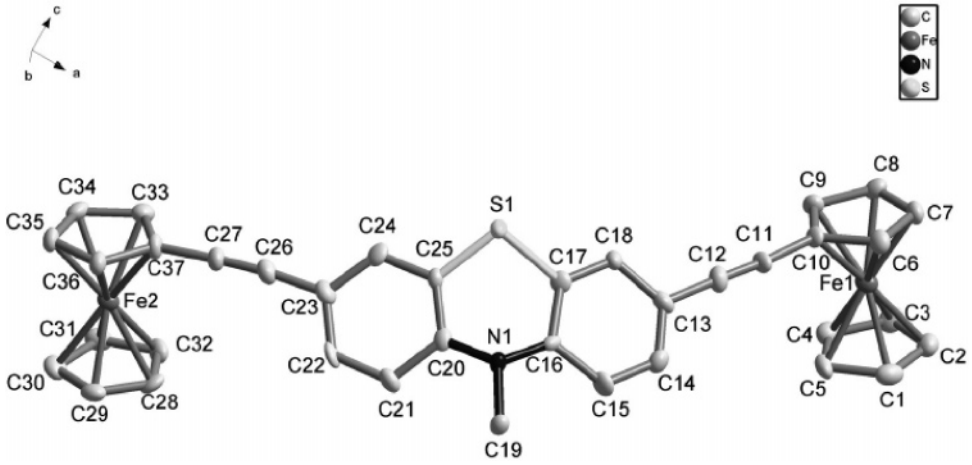

Figure 2. ORTEP diagram of **2**·H_2O with ellipsoids drawn at the 30% probability level. Hydrogen and oxygen atoms are omitted for clarity.

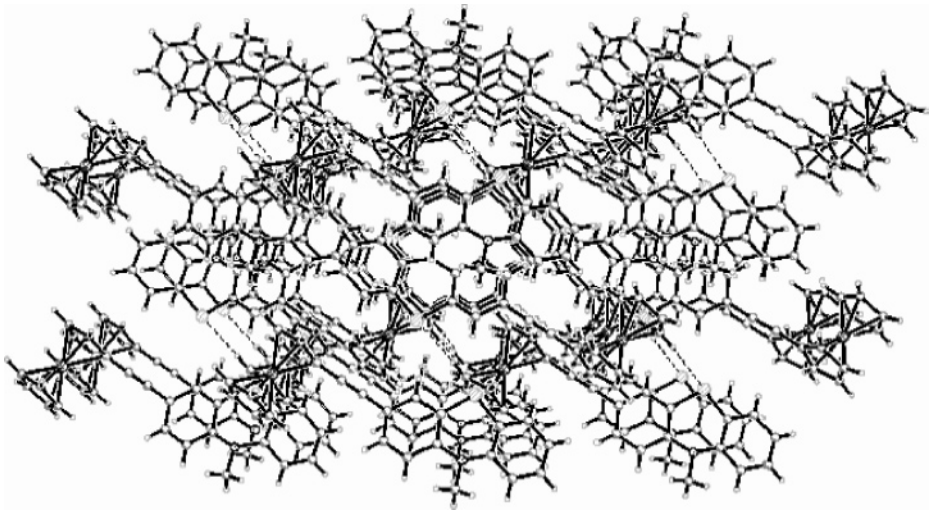

Figure 3. Crystal packing of **1**, showing the C−H···S hydrogen bonds (dashed lines) along the *a* axis with ellipsoids drawn at the 50% probability level.

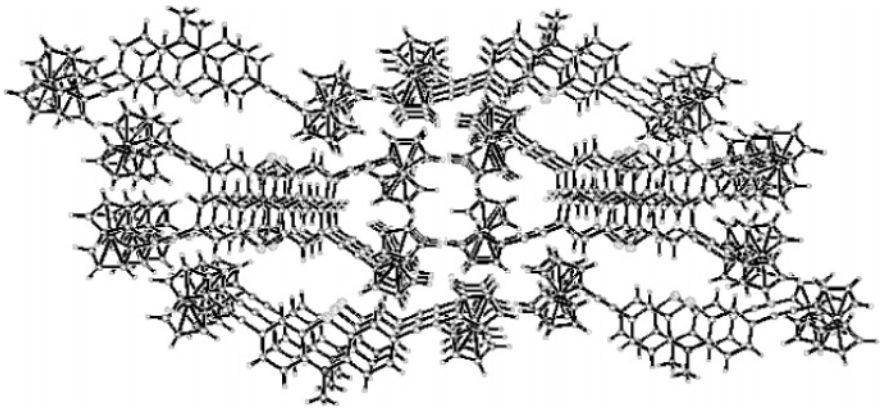

Figure 4. Crystal packing of **2**, showing the C−H···S hydrogen bonds (dashed lines) along the *b* axis with ellipsoids drawn at the 50% probability level.

MPT coupling in the ground state of **2**, which is demonstrated by DFT calculations discussed later. In the crystal packing along the *b* axis, as shown in Figure 4, adjacent molecules in **2** are stacked in an inverse fashion through strong offset $\pi\cdots\pi$ aromatic stacking interactions, with a face-to-face distance of 3.758 Å. C(19)−H(19)···S(1) hydrogen bonds also exist between molecules with an S···H separation of 2.860 Å (clearly shown in the Supporting Information). Therefore, supramolecular interactions, including $\pi\cdots\pi$ stacking and C−H···S hydrogen bonds, generate a unique supramolecular architecture in the solid state of **2**.

3.3. Electronic Properties. The solution-phase UV−vis absorption spectra of **1** and **2** were recorded at room temperature. The absorption spectra reported in Figure 5 are dominated in the UV−visible region by absorption features at about 270, 300, 330−370, and 440−480 nm, which are given in Table 3. Weak solvatochromism is observed in the absorption bands for both complexes. Generally, these bands can be assigned to $\pi \rightarrow \pi^*$, ICT (intramolecular charge transfer), and MLCT (metal-to-ligand charge transfer) transitions.[7e,16,17,18c] The computational study discussed later will give a detailed band assignment.

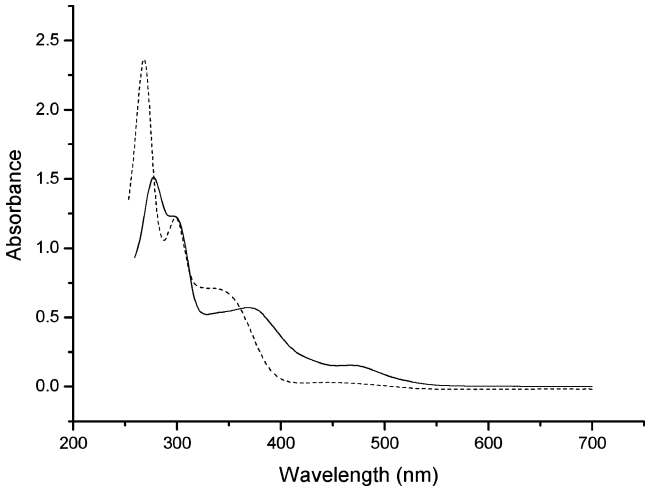

Figure 5. UV−vis absorption spectra of complexes **1** (5.7×10^{-5} mol/L, dashed line) and **2** (3.1×10^{-5} mol/L, solid line) in dichloromethane at room temperature.

The main difference in the absorption spectra of these two compounds is that both MLCT and $\pi \rightarrow \pi^*$ transitions of **2** are strongly bathochromically shifted compared with those of **1**. Moreover, the oscillator strengths (ϵ_{max}) of all the bands of **2** are larger than those of **1**, suggesting a higher probability for

(16) (a) Kulkarni, A. P.; Wu, P.-T.; Kwon, T. W.; Jenekhe, S. A. *J. Phys. Chem. B* **2005**, *109*, 19584. (b) Sailer, M.; Nonnenmacher, M.; Oeser, T.; Müller, T. J. J. *Eur. J. Org. Chem.* **2006**, 423.

(17) (a) Lai, R. Y.; Fabrizio, E. F.; Lu, L.; Jenekhe, S. A.; Bard, A. J. *J. Am. Chem. Soc.* **2001**, *123*, 9112. (b) Lai, R. Y.; Kong, X.; Jenekhe, S. A.; Bard, A. J. *J. Am. Chem. Soc.* **2003**, *125*, 12631.

(18) (a) Knorr, A.; Daub, J. *Angew. Chem., Int. Ed. Engl.* **1995**, *34*, 2664. (b) Kong, X.; Kulkarni, A. P.; Jenekhe, S. A. *Macromolecules* **2003**, *36*, 8992. (c) Kurosawa, M.; Nankawa, T.; Matsuda, T.; Kubo, K.; Kurihara, M.; Nishihara, H. *Inorg. Chem.* **1999**, *38*, 5113.

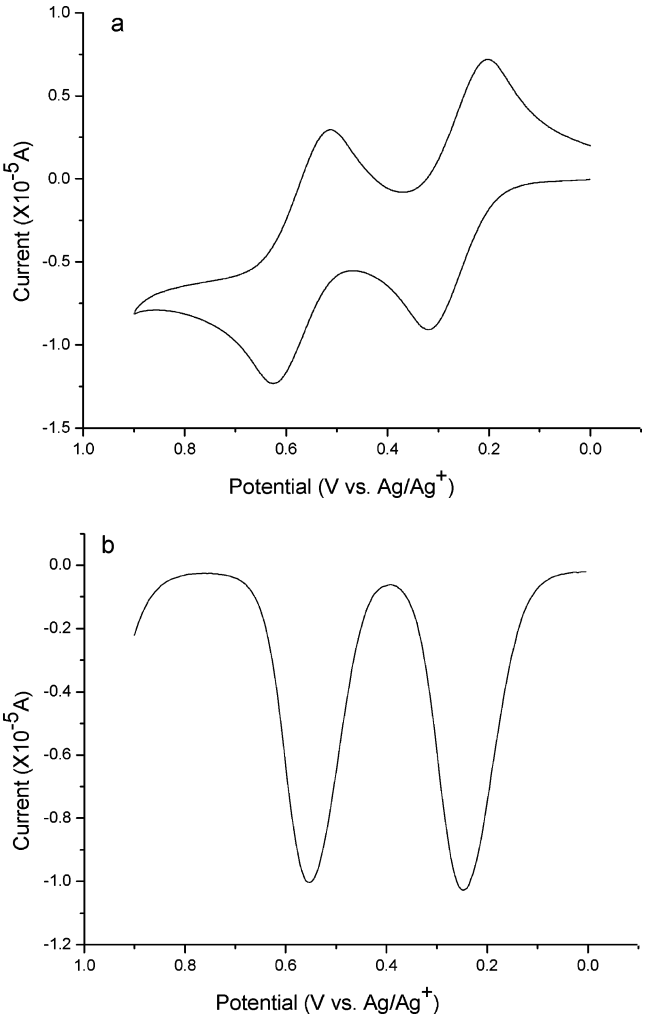

Figure 6. Cyclic voltammogram (a) and differential pulse voltammogram (b) of complex **1** in acetonitrile (20 °C, 1.1 mM of **1**, 0.1 M TBAP, Pt disk as a working electrode, Ag/Ag^+ as a reference electrode, and Pt wire as a counter electrode, scan rate 100 mV/s).

Table 3. UV−Vis Absorption Properties of 1 and 2 in Solvents of Varying Polarity

solvent	λ_{max}^{abs} (nm) (ϵ (10^4 M^{-1} cm^{-1}))
	Complex **1**
CH_2Cl_2	268 (4.1), 299 (2.1), 335 (1.2), 441 (0.052)
CH_3CN	267 (4.4), 296 (2.3), 334 (1.3), 441 (0.064)
	Complex **2**
toluene	301 (4.0), 368 (1.7), 468 (0.51)
CH_2Cl_2	277 (4.8), 300 (3.9), 368 (1.8), 467 (0.50)
$CHCl_3$	275 (5.1), 299 (4.3), 364 (1.9), 467 (0.52)
CH_3CN	275 (5.0), 297 (4.1), 361 (1.8), 467 (0.51)

CT (ICT and MLCT) and $\pi \rightarrow \pi^*$ transitions in **2**.[17] All of these facts indicate a better electronic coupling between the Fc and MPT subunits and a larger π-conjugative effect in **2**. Actually, the better coplanarity between MPT and Fc moieties (vide supra) and the more conjugative subunits in **2** leads to a more remarkable π-electron delocalization and a greater π-conjugation.

3.4. Electrochemical Properties. The electrochemical properties of complexes **1** and **2** were measured by cyclic voltammograms (CV) and differential pulse voltammetry (DPV). Parts a and b of Figure 6 show the CV and DPV of **1** in the 0.0−0.9 V (vs Ag/Ag^+) scanning range, respectively. The first reversible one-electron oxidation at 0.248 V vs Ag/Ag^+ is derived from the ferrocenyl core, and the second reversible one-electron oxidation at 0.552 V vs Ag/Ag^+ is attributed to the phenothiazinyl moiety in comparison with the Fc and MPT parent system (Fc and MPT undergo oxidative processes at 0.072 and 0.412 V vs Ag/Ag^+, respectively). This is also supported by DFT calculations on **1**, where the orbital coefficient in the HOMO-1 is predominantly ferrocenyl centered and that in the HOMO is phenothiazinyl centered (vide infra). Therefore, these two 1e oxidative processes can be assigned to the formation of a ferrocenium ion and a phenothiazinyl radical cation.[17,18] Upon oxidation to higher potentials, complex **1** exhibits another irreversible oxidative peak at about 1.1 V vs Ag/Ag^+ at a scan rate of 100 mV/s, and at the same time, the former two reversible oxidations also become irreversible. The irreversibility of the third oxidative wave at higher potential likely stems from the highly reactive nature of the dication of the phenothiazine moiety.[17]

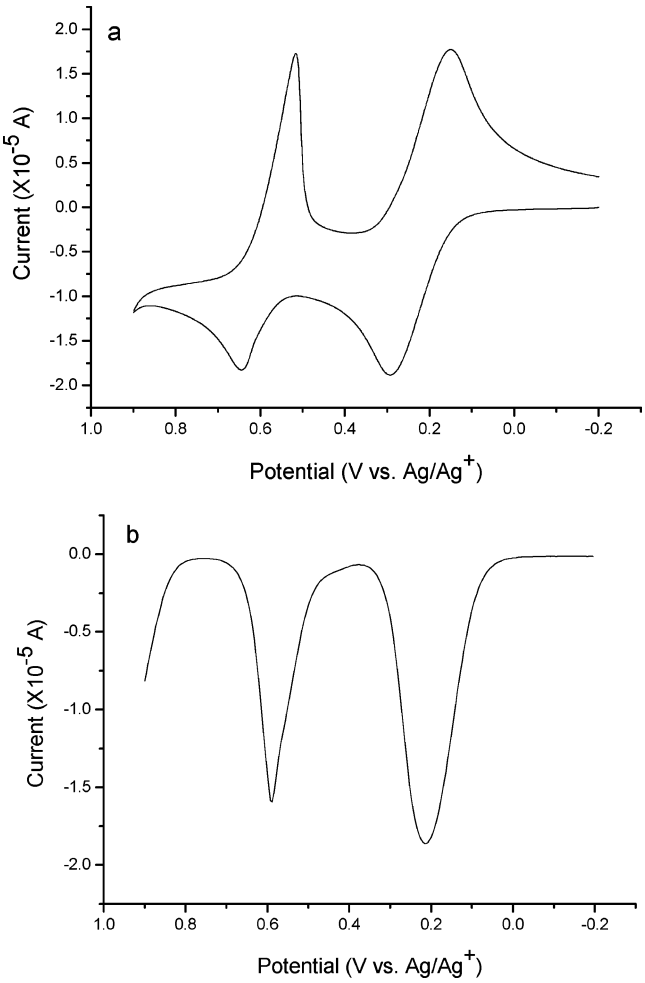

Figure 7. Cyclic voltammogram (a) and differential pulse voltammogram (b) of complex **2** in acetonitrile (20 °C, 1.0 mM of **2**, 0.1 M TBAP, Pt disk as a working electrode, Ag/Ag^+ as a reference electrode, and Pt wire as a counter electrode, scan rate 100 mV/s).

The CV and DPV measurements of complex **2** are displayed in Figure 7. In the scan range of −0.2 to 0.9 V (vs Ag/Ag^+), **2** also undergoes two steps of oxidation, in which the area ratio of the first wave at 0.216 V vs Ag/Ag^+ to the second one at 0.588 V vs Ag/Ag^+ is nearly 2. Therefore, the two metallocene centers in **2** are electronically decoupled; the first, simultaneously undergoing reversible 1e oxidation at lower potential, is ferrocenyl-centered, as expected, while the second quasi-reversible 1e oxidation at higher potential is, as expected, phenothiazinyl-centered.[17,18] This is also supported by DFT calculations on **2**, where the orbital coefficient in the HOMO-1 is predominantly ferrocenyl-centered and that in the HOMO is

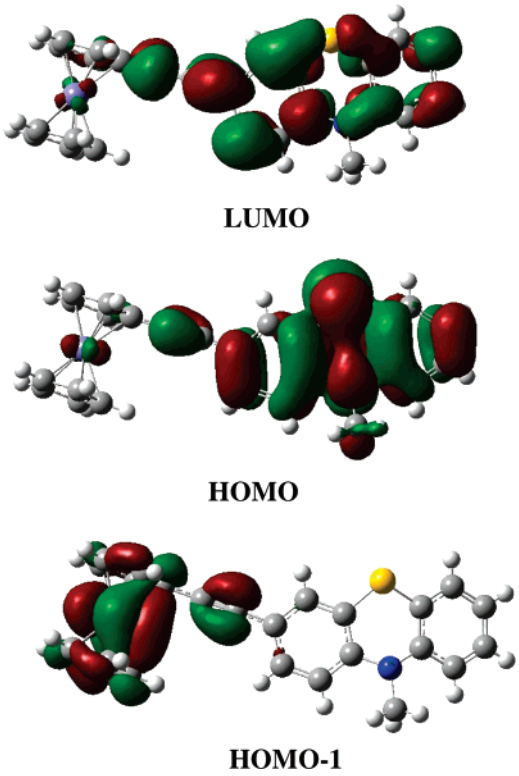

Figure 8. LUMO, HOMO, and HOMO-1 orbitals of **1**.

phenothiazinyl-centered (vide infra). Similar to the case for complex **1**, upon scanning to more positive potentials at a scan rate of 100 mV/s, the former two couples of reversible waves also exhibit irreversibility after the formation of the highly reactive dication of the phenothiazine moiety.[17]

In a comparison of complexes **1** and **2**, the difference in the first oxidation can be attributed not only to stereoelectronic effects but also to π-conjugative effects. On the one hand, as a consequence of a much more significant torsion of the phenothiazinyl moiety from coplanarity with the Cp rings in complex **1** than in complex **2** (vide supra), π-orbital overlap is decreased in **1** and thus the more negative inductive effect of the heteroaromatic substituent leads to an anodic shift of the first ferrocenyl-centered oxidation to higher potential. On the other hand, besides the fact that better coplanarity in complex **2** favors the π-orbital overlap and the orbital mixing, there is evidence that the greater π-conjugative effect between the two ferrocenyl subunits and one phenothiazinyl subunit also causes the first ferrocenyl-centered oxidation to a cathodic shift of lower potential. For the second oxidation, however, the case is just the opposite. In comparison to that in complex **1**, the subsequent oxidation of the phenothiazinyl moiety in complex **2** is shifted anodically as a consequence of the two adjacent electron-withdrawing ferrocenium substituents. This result also suggests that the electronic communication between ferrocene and phenothiazine in the dication state of complex **2** is stronger than in the monocation state of complex **1**.[19]

3.5. Quantum-Chemical Calculations. The optical and electronic properties of these two conjugated complexes have been theoretically investigated by means of density functional theory (DFT) and time-dependent DFT (TDDFT) calculations at the molecular level. Figures 8 and 9 show the plots of the most representative molecular frontier orbitals in the ground states of **1** and **2**, respectively. Other frontier orbitals relevant to discussion are available as Supporting Information. In both molecules, the HOMO's and LUMO's are nearly completely localized between the MPT moiety and the ethynyl bridge, while the HOMO-1's are almost predominately localized between the Fc moiety and the ethynyl bridge. The Fc characteristic HOMO-1 and the MPT characteristic LUMO indicate that the HOMO-1 → LUMO absorption transition bears a significant intramolecular charge-transfer (ICT) character, while the HOMO → LUMO absorption transition dominantly between the MPT characteristic orbitals suggests that this kind of transition is of $\pi \rightarrow \pi^*$ character. The most representative calculated optical transitions for them are collected in Table 4. For both complexes, the calculated transitions qualitatively agree with the experi-

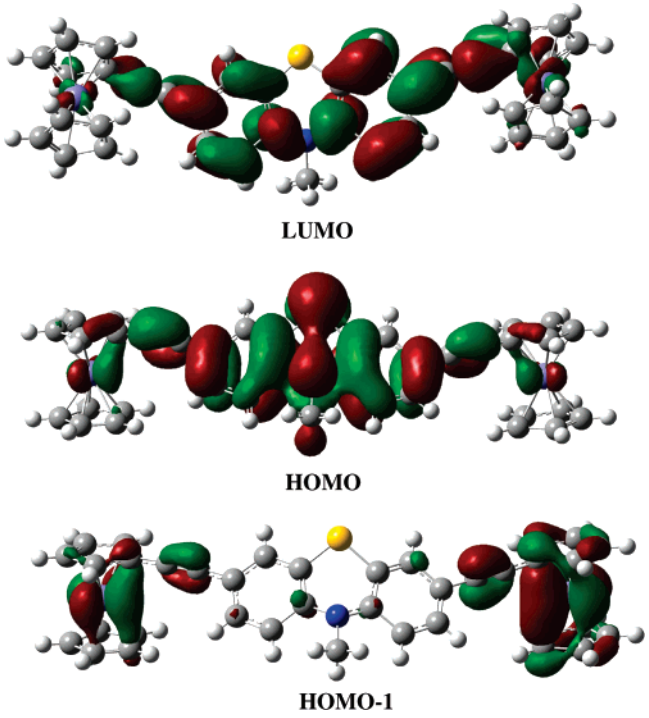

Figure 9. LUMO, HOMO, and HOMO-1 orbitals of **2**.

Table 4. Main Calculated Optical Transitions for 1 and 2

calcd (nm)	f^a	composition (%)	character	exptl (nm)
		Complex **1**		
452.25	0.0009	39 (HOMO−4 → LUMO+3)	MLCT	441
		28 (HOMO−2 → LUMO+5)	MLCT	
		17 (HOMO−5 → LUMO+3)	MLCT	
350.30	0.0869	97 (HOMO → LUMO)	$\pi \rightarrow \pi^*$	335
318.77	0.0834	87 (HOMO → LUMO+1)	$\pi \rightarrow \pi^*$	
307.48	0.1274	86 (HOMO → LUMO+2)	$\pi \rightarrow \pi^*$	299
300.95	0.0010	100 (HOMO−1 → LUMO)	ICT	
294.14	0.0311	100 (HOMO−2 → LUMO)	ICT	
		Complex **2**		
460.06	0.0026	54 (HOMO−8 → LUMO+3/ LUMO+5/LUMO+6/LUMO+7/ LUMO+8/LUMO+9)	MLCT	467
		22 (HOMO−4 → LUMO+3/ LUMO+4/LUMO+5/LUMO+6)	MLCT	
		11 (HOMO−3 → LUMO+4)	MLCT	
357.57	0.3998	100 (HOMO → LUMO)	$\pi \rightarrow \pi^*$	368
336.98	0.0239	93 (HOMO → LUMO+1)	$\pi \rightarrow \pi^*$	
323.29	0.0694	85 (HOMO → LUMO+2)	$\pi \rightarrow \pi^*$	300
302.41	0.0550	87 (HOMO−1/HOMO−2/ HOMO−3 → LUMO)	ICT	
301.15	0.0197	76 (HOMO−2/ HOMO−3 → LUMO)	ICT	

[a] Oscillator strength.

(19) Sailer, M.; Rominger, F.; Müller, T. J. J. *J. Organomet. Chem.* **2006**, *691*, 299.

Table 5. Calculated DFT Energy Levels of Frontier Orbitals (eV), E_g (HOMO−LUMO Band Gap; eV), E_g' (HOMO-1−LUMO Band Gap; eV), and Ground-State Dipole Moments (D) of Complexes 1 and 2, MPT, and Fc

						atomic charge		
complex	LUMO	HOMO	HOMO-1	E_g	E_g'	N	S	dipole moment
1	−0.8923	−5.1525	−5.5430	4.2602	0.2905	−0.5385	0.1856	
2	−1.0683	−5.1691	−5.5236	4.1008	0.3545	−0.5847	0.1957	3.2452
MPT[16]	−0.32	−5.03		4.71				
Fc[20]	−0.32	−5.54	−6.31	5.22				

mental ones. As for complex **1**, the lowest energy band experimentally found at 442 nm with a lower value of ϵ corresponds to the transition calculated at 452 nm with low oscillator strength *f*. This band mainly originates from several transitions of HOMO-4/HOMO-5 to LUMO+3 and HOMO-2 to LUMO+5, which can be assigned to MLCT due to the orbital characters of the corresponding starting and arriving states (see the Supporting Information). At shorter wavelength, an intense and broad band found at 335 nm may be related to two calculated intense bands at 350 and 319 nm, which come from HOMO to LUMO and HOMO to LUMO+1 transitions, respectively. HOMO, LUMO, and LUMO+1 orbitals are mainly MPT localized; thus, the absorption band at 335 nm is of $\pi \rightarrow \pi^*$ character. A more intense experimental 299 nm band appears to be related to a $\pi \rightarrow \pi^*$ transition at 307 nm and ICT transitions at 301 nm and 294 nm. The $\pi \rightarrow \pi^*$ transition originates from HOMO to LUMO+2, while the ICT transitions are from HOMO-1 to LUMO and HOMO-2 to LUMO, respectively. As for complex **2**, similar results can be obtained from a TDDFT study. The characteristic bands of **2** are explained as follows. The experimental absorption band of 467 nm at longer wavelength is of MLCT character, relevant to the calculated band at 460 nm composed of a set of mixed MLCT transitions between different orbitals listed in Table 4. The large broad band found at 368 nm belongs to a $\pi \rightarrow \pi^*$ transition originating from HOMO to LUMO transfer calculated at 358 nm and HOMO to LUMO+1 calculated at 337 nm. The experimentally found band of 300 nm with strong oscillator strength can be analyzed as a combination of $\pi \rightarrow \pi^*$ and ICT transitions, where the $\pi \rightarrow \pi^*$ transition mainly comes from HOMO to LUMO+2 calculated at 323 nm and the ICT transitions come from HOMO-1/HOMO-2/HOMO-3 coupled to the LUMO calculated at 302 and 301 nm, respectively. Therefore, the calculated absorption bands in these compounds are in excellent agreement with the experimental values.

Furthermore, as shown in Figures 8 and 9, the frontier orbitals in complex **2** extend beyond the ferrocenyl moieties, which may lead to better π-electron delocalization. This finding is identical with the results of higher oscillator strength of the absorption bands in complex **2** (vide supra).

The calculated LUMO, HOMO, and HOMO-1 energy levels of the two molecules together with their parent building blocks of MPT and Fc are given in Table 5. The ferrocenyl-centered HOMO-1 levels for complexes **1** and **2** are −5.5430 and −5.5236 eV, respectively, which are very close to the HOMO level of Fc (−5.54 eV).[20] The phenothiazinyl-centered HOMO levels for them are −5.1525 and −5.1691 eV, respectively, which are very close to the HOMO level of MPT (−5.03 eV).[16] All of the above confirms the previously discussed hypothesis of the two consecutive couples of site-selective oxidations occurring on the ferrocenyl and phenothiazinyl moieties in the electrochemistry. Moreover, the slightly higher HOMO-1 energy level in complex **2** and HOMO energy level in complex **1** are in agreement with the results of easier ferrocenyl oxidation of **2** and phenothiazinyl oxidation of **1**. Meanwhile, the theoretically predicted HOMO-1−HOMO gaps (0.2905 eV for **1**; 0.3545 eV for **2**) are in excellent agreement with those experimentally estimated from electrochemistry, which are 0.304 eV for **1** and 0.372 eV for **2**. Therefore, the DFT calculations predict the experimentally observed trends in the redox properties of these two complexes very well.

The calculated HOMO−LUMO gaps (E_g) for conjugative π-electron extending molecules **1** and **2** are 4.2602 and 4.1008 eV, respectively, which are both lower than for the parent blocking compounds MPT and Fc. These data deviate from the values derived from the experimentally estimated optical band gaps (3.7010 eV for **1**; 3.3691 eV for **2**), since only the ground states were taken into consideration in the MO calculations. Moreover, the extensive transverse interactions, such as $\pi\cdots\pi$ stacking and C−H···S hydrogen bonding, existing in the real solid state, play an essential role in decreasing the HOMO−LUMO gaps.[21] In addition, it is worth mentioning that the trend of the two calculated HOMO−LUMO gaps is in accordance with the experimental results. The lower E_g value of **2**, compared to that of **1**, may be the result of the larger delocalization and conjugative effect of **2**, in which both LUMO and HOMO frontier orbitals extend beyond the ferrocenyl moiety, as clearly seen in Figures 8 and 9. This may be attributed to the better coplanarity of **2**, shown by single-crystal X-ray diffraction. In addition, the atomic charges of N and S in **1** are −0.5385 and 0.1856, respectively, and those in **2** are −0.5847 and 0.1957, respectively. The larger difference between the atomic charges of N and S in **2** may contribute to the higher ground-state dipole moment of **2** (3.2452 D) relative to that of **1** (2.6623 D). Overall, these initial DFT and TDDFT calculations on the two complexes provide deep insight into their electronic structures and properties.

4. Conclusions

In summary, organometallic−organic hybrid electrophores containing ferrocene and phenothiazine units have been successfully synthesized by Sonogashira coupling reactions. Structural effects on their photophysical and electrochemical properties have been investigated. Single-crystal X-ray diffraction studies indicate that the coplanarity of the two building blocks (ferrocene and phenothiazine moieties) in complex **2** is better than that in complex **1**, which may lead to better π-electron delocalization and stronger optical absorption in **2**. Intermolecular hydrogen bonding and π-stacking interactions are displayed in these oligomeric ferrocene−phenothiazine systems. In particular, DFT and TDDFT calculations have allowed a detailed understanding of the electronic structure and absorption spectra of the two complexes. Quantum-chemical calculations

(20) Schreckenbach, G. *J. Phys. Chem.* **1999**, *110*, 11936.

(21) (a) Zheng, S.-L.; Zhang, J.-P.; Chen, X.-M.; Huang, Z.-L.; Lin, Z.-Y.; Wong, W.-T. *Chem. Eur. J.* **2003**, *9*, 3888. (b) Zheng, S.-L.; Zhang, J.-P.; Wong, W.-T.; Chen, X.-M. *J. Am. Chem. Soc.* **2003**, *125*, 6882. (c) Huang, X.-C.; Zheng, S.-L.; Zhang, J.-P.; Chen, X.-M. *Eur. J. Inorg. Chem.* **2004**, 1024.

showed that LUMO's and HOMO's are highly phenothiazine localized, whereas HOMO-1's are highly ferrocene centered, and better π-electron conjugation is found in the frontier orbitals of complex **2**. The different coplanarities, π-electron conjugations, and DFT-calculated energy levels of frontier orbitals and HOMO−LUMO energy gaps of the two complexes are in excellent agreement with their experimental photophysical and electrochemical results. Future studies will address the properties of the molecule-based systematic Fc−MPT materials as molecular wires and molecular switches as well as molecular rectifiers in emerging molecular electronics.

Acknowledgment. We are grateful for financial support from the Foundation of China Scholarship Council (No. 0205133143), the State Key Laboratory of Coordination Chemistry, and the Center of Analysis and Determining of Nanjing University (No. 0205001380).

Supporting Information Available: CIF files giving X-ray crystallographic data and figures of the crystal packing, showing the intermolecular C−H···S hydrogen-bonding interactions, and plots of the frontier orbitals. This material is available free of charge via the Internet at http://pubs.acs.org.

OM060923O